



HAL
open science

Dissipative polarization domain walls in a passive driven Kerr resonator

Bruno Garbin, Julien Fatome, Gian-Luca Oppo, Miro Erkintalo, Stuart G
Murdoch, Stéphane Coen

► **To cite this version:**

Bruno Garbin, Julien Fatome, Gian-Luca Oppo, Miro Erkintalo, Stuart G Murdoch, et al.. Dissipative polarization domain walls in a passive driven Kerr resonator. *Physical Review Letters*, 2021, 126 (2), 10.1103/physrevlett.126.023904 . hal-03142276

HAL Id: hal-03142276

<https://hal.science/hal-03142276>

Submitted on 15 Feb 2021

HAL is a multi-disciplinary open access archive for the deposit and dissemination of scientific research documents, whether they are published or not. The documents may come from teaching and research institutions in France or abroad, or from public or private research centers.

L'archive ouverte pluridisciplinaire **HAL**, est destinée au dépôt et à la diffusion de documents scientifiques de niveau recherche, publiés ou non, émanant des établissements d'enseignement et de recherche français ou étrangers, des laboratoires publics ou privés.

Dissipative polarization domain walls in a passive driven Kerr resonator

Bruno Garbin,^{1,2,3} Julien Fatome,^{1,2,4} Gian-Luca Oppo,⁵
Miro Erkintalo,^{1,2} Stuart G. Murdoch,^{1,2} and Stéphane Coen^{1,2,*}

¹*Physics Department, The University of Auckland,
Private Bag 92019, Auckland 1142, New Zealand*

²*The Dodd-Walls Centre for Photonic and Quantum Technologies, Dunedin, New Zealand*

³*Université Paris-Saclay, CNRS, Centre de Nanosciences et de Nanotechnologies, 91120, Palaiseau, France*

⁴*Laboratoire Interdisciplinaire Carnot de Bourgogne (ICB),
UMR 6303 CNRS, Université de Bourgogne Franche-Comté,
9 Avenue Alain Savary, BP 47870, F-21078 Dijon, France*

⁵*SUPA and Department of Physics, University of Strathclyde, Glasgow G4 0NG, Scotland, European Union*

Using a passive driven nonlinear optical fiber ring resonator, we report the experimental realization of dissipative polarization domain walls. The domain walls arise through a symmetry breaking bifurcation and consist of temporally localized structures where the amplitudes of the two polarization modes of the resonator interchange, segregating domains of orthogonal polarization states. We show that dissipative polarization domain walls can persist in the resonator without changing shape. We also demonstrate on-demand excitation, as well as pinning of domain walls at specific positions for arbitrary long times. Our results could prove useful for the analog simulation of ubiquitous domain-wall related phenomena, and pave the way to an all-optical buffer adapted to the transmission of topological bits.

Domain walls (DWs) are self-localized kink-type topological defects that connect two stable states of a physical system. They usually form in the presence of a spontaneous symmetry breaking bifurcation [1], and are found in a variety of contexts, including magnetism [2], hydrodynamics [3], biology [4], Bose-Einstein condensates [5], and string theory [6]. The paradigmatic examples are the interfaces that separate domains with distinct magnetization in ferromagnetic materials [2, 7], whose unique properties are exploited in modern spintronics devices to store or even transfer information [8]. Additionally, DWs are central to numerous phase transitions in condensed matter and quantum physics [4, 9].

DWs are also known to manifest themselves in optical systems. In this context, the terminology was first used to describe stationary spatial distributions of light arising from the pure nonlinear (Kerr) interactions of counter-propagating beams [10] (and reported experimentally in [11]). Subsequently, Haelterman and Shepard introduced the concept of DW *solitons* by describing vector, kink-type propagating structures, segregating homogeneous domains of orthogonal polarization states, and that resist diffractive (transverse) or dispersive (temporal) spreading in Kerr media [12]. Referred to as polarization DWs (or PDWs), these structures have only recently been convincingly observed experimentally by Gilles et al — more than two decades after their theoretical description — in the single-pass, *conservative*, propagation configuration of a normally dispersive single-mode optical fiber [13]. Remarkably, this experiment has demonstrated the potential of temporal PDWs for transmission of topological bits, robust to noise and nonlinear impairments, as originally foreseen [14].

Here we extend the work of Gilles et al [13] by imple-

menting all-optical storage of temporal PDWs. This is obtained by taking advantage of spontaneous symmetry breaking in an externally-driven passive Kerr ring resonator, enabling recirculation of PDWs [15]. To date, such *dissipative* PDWs have not been observed experimentally. Our demonstration constitutes a key technology in supporting potential topologically-robust transmissions. It could also pave the way to real-time, stochastic, room temperature analog simulations of DW-related solid-state physics phenomena not easily observable in other settings [16–18]. Finally, dissipative PDWs are also related to phase DWs predicted in the transverse structure of optical parametric [19] and four-wave mixing [20] oscillators. As the dynamics of these systems can be used to estimate the ground state of the Ising Hamiltonian [21, 22], domains of orthogonal polarizations segregated by dissipative PDWs could be associated with different spin states and provide a new route to solve complex optimization problems. We note that hints of dissipative PDW “complexes” have been reported in fiber lasers, but these observations have proved hard to interpret [23–25]. In contrast, the results we present in this Letter provide the first clear signature of isolated dissipative temporal PDWs.

We start by describing theoretically how dissipative PDWs emerge in our system. We consider a dispersive passive ring resonator that is externally and coherently driven by a continuous-wave (cw) light beam and that exhibits a Kerr nonlinearity. The intracavity field is described in terms of the complex amplitudes, $E_{1,2}$, of the two orthogonal polarization modes of the resonator. In the mean-field limit, the temporal evolution of these two modal amplitudes can be described by normalized cou-

pled Lugiato-Lefever equations as [26–29],

$$\frac{\partial E_{1,2}}{\partial t} = \left[-1 + i(|E_{1,2}|^2 + B|E_{2,1}|^2 - \Delta) - i\frac{\partial^2}{\partial \tau^2} \right] E_{1,2} + \sqrt{X/2}. \quad (1)$$

The terms on the right hand side of these equations describe respectively cavity losses, self- and cross-phase modulation, the cavity phase detuning, chromatic dispersion (taken as normal, to avoid modulational instabilities of cw stationary states of the resonator [27]), and external driving. We consider here identical detuning and driving strength for the two modes. t represents a slow time over which the evolution of the intracavity field takes place, at the scale of the cavity photon lifetime, while τ is a fast-time that describes the temporal structure of the field along the round trip of the resonator. B is the cross-phase modulation coefficient. In optical fibers (as used in our experiments discussed below), B can be as large as 2 for circularly polarized modes [30], but PDWs continue to exist so long as $B > 1$ [12]. Finally, Δ is the detuning parameter, which measures the separation between the driving laser frequency and the nearest cavity resonance in terms of the cavity half-linewidth, and X is the normalized total driving power.

Representative stationary ($\partial/\partial t = 0$) cw ($\partial/\partial \tau = 0$) solutions of the above equations are illustrated in Fig. 1(a). Because the equations are symmetric with respect to an interchange of the two polarization modes, $E_1 \rightleftharpoons E_2$, the simplest stationary solutions express this symmetry ($E_1 = E_2$). Here we retrieve the characteristics S-shaped, bistable response of the Kerr cavity [yellow curve in Fig. 1(a)]. However, above a certain threshold of driving power, the upper-state solution undergoes a spontaneous symmetry breaking (SSB): the intensity of the two polarization modes part (blue and orange curves) [27, 31, 32]. Because of the symmetry of the system, there exists two such solutions, mirror-images of each other, in which a different mode dominates. These solutions correspond to intracavity fields that are overall elliptically polarized, with opposite handedness. This polarization SSB has been recently observed experimentally [33]. When the two symmetry-broken solutions are simultaneously excited in different regions (or domains) of the resonator, there exists a shape-preserving temporal structure interconnecting them and across which the two polarization modes interchange: the PDW [Fig. 1(b)]. Note how the total intensity (black curve) is nearly constant across the PDW. As shown numerically in [15], these dissipative PDWs can circulate indefinitely around the driven resonator without losing power or changing shape. Their robustness stems from a double balance, similar to that realized for temporal cavity solitons [34]: the external driving compensates the losses, while dispersive spreading is balanced by the nonlinearity. The latter

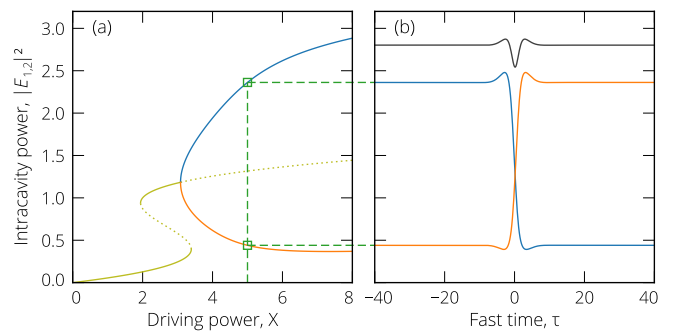


FIG. 1. Numerical illustration of the polarization SSB and associated PDWs for $\Delta = 3$ and $B = 2$ as described by Eqs. (1). (a) Stationary cw solutions, $|E_1|^2$ and $|E_2|^2$, versus driving power X . The yellow curve represents symmetric solutions ($E_1 = E_2$; dotted lines are unstable states) while the blue and orange curves represent asymmetric solutions ($E_1 \neq E_2$). (b) Temporal intensity profile of a single PDW connecting the two cw symmetry-broken solutions existing for $X = 5$. Blue and orange curves correspond to the two polarization modes, while the black curve shows the total power.

occurs through the same mechanism as for the conservative PDWs described by Haelterman and Sheppard [12].

The experimental setup that we have used to realize and control dissipative PDWs is depicted in Fig. 2. It is based on a $\simeq 10$ m-long passive optical fiber ring resonator mostly built out of highly nonlinear, normal dispersion, “spun” fiber, exhibiting very low birefringence due to twisting applied at the drawing stage [35]. The ring is closed with two SMF-28 fiber couplers, with splitting ratio 90/10 and 99/1, enabling injection of the driving and monitoring of the intracavity field, respectively. Overall the resonator exhibits normal dispersion at the 1550-nm driving wavelength, with averaged second order dispersion coefficient $\langle \beta_2 \rangle \simeq 53$ ps²/km and nonlinear coefficient $\langle \gamma \rangle \simeq 4.3$ W⁻¹ km⁻¹. The free-spectral-range is found to be 19.8 MHz, corresponding to a round-trip time t_R of 50.6 ns. The measured finesse is about 24, amounting to losses of 26% per round-trip, a photon lifetime of about $4 t_R$, and a resonance width of 825 kHz.

The resonator is synchronously driven with flat-top 1.1 ns pulses [36]. These pulses are obtained by carving the cw output of a 1 kHz linewidth, erbium-doped distributed-feedback fiber laser with a 10 GHz-bandwidth Mach-Zehnder amplitude modulator (AM). The AM is followed by a fast polarization modulator (PM) used to apply perturbations to the driving polarization as explained below. The two modulators are connected to separate pattern generators (PG) synchronized to the same $\simeq 10$ GHz sinusoidal clock, set at a harmonic of the FSR. Before injection into the resonator, the driving pulses are amplified up to 15 W peak power (corresponding to X values up to 30) using an erbium-doped fiber amplifier (EDFA) combined with a band-pass filter (BPF) for rejection of amplified spontaneous emission

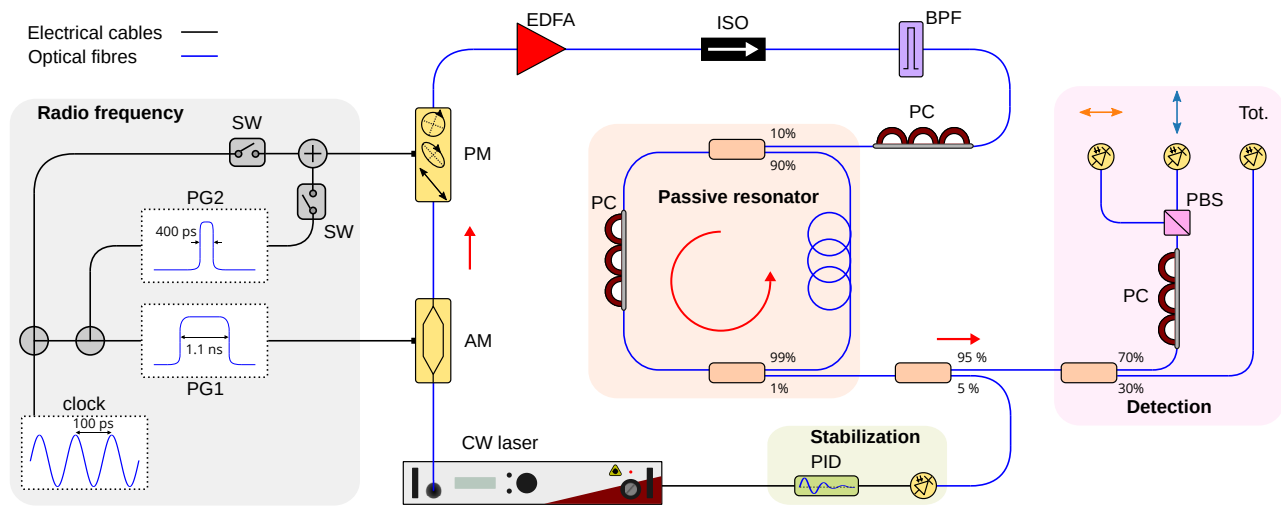


FIG. 2. Experimental set-up. The passive fiber ring resonator is highlighted with an orange background. CW laser, driving laser; AM, Mach-Zehnder amplitude modulator; PM, polarization modulator; clock, signal generator; PG1 and PG2, pattern generators; SW, electrical switch; EDFA, erbium-doped fibre amplifier; ISO, optical isolator; BPF, band-pass filter; PC, polarization controller; PBS, polarizing beamsplitter.

noise. At the output, we monitor separately the power of the two polarization modes, split by a polarizing beamsplitter (PBS) preceded by a polarization controller (PC), as well as the total output power. These three signals are measured with a triplet of 12.5 GHz-bandwidth amplified photodiodes. Additionally, a small fraction of the total output power is monitored and maintained constant by a PID feedback controller acting on the driving laser frequency, for stabilization of the detuning with respect to environmental fluctuations.

PDWs require interchange symmetry between the two polarization modes of the resonator. Our optical fiber ring is however slightly birefringent, due to the couplers, which are not built out of spun fiber, as well as unavoidable fiber bending. To counterbalance the residual cavity birefringence, a PC is incorporated into the fiber ring. In this configuration, the polarization modes are associated with states of polarization that evolve around the fiber ring, and that map onto themselves over one round-trip [37]. This evolution is averaged in the mean-field model, Eqs. (1) [29]. Another PC, inserted before the input coupler, is used to project the driving field equally onto the two modes, and realize balanced driving conditions.

In practice, the setup is adjusted by observing the resonances of the two polarization modes while scanning the driving laser frequency. A position of the intracavity PC is found for which, close to a point where the resonances overlap, their separation can be tuned without affecting their relative amplitudes. With the two resonances slightly apart, i) the output PC is set to correctly separate the modes in the detection stage, and ii) driving is balanced by matching the amplitudes of the observed resonances. Birefringence is then cancelled by superimposing the two resonances. Finally, we increase

the driving power until we observe the polarization SSB described in Fig. 1(a) (and reported in [33]), and we lock the detuning within the region where SSB occurs.

To proceed with observations of PDWs, we record the output power levels across our driving pulses over subsequent cavity round-trips using a 13-GHz-bandwidth real-time oscilloscope. A typical evolution is shown as color plots (bottom-to-top) in Figs. 3(a)–(c), with the three panels corresponding respectively to the powers of the two separate polarization modes and their total. Using matching colors, line plots are also presented in Fig. 3(d) for selected round trips. As can be seen, we start in a symmetry-broken state, where the “orange” mode uniformly dominates; see round trip #500 in panel (d). After about 1000 cavity round-trips, a localized, 400 ps-wide, rf perturbation is applied for about 20 round-trips to the PM. In this way, we carve a domain of different polarization in the middle of the driving pulse. We then let the intracavity field evolve freely for the rest of the measurement. Shortly after applying the perturbation, we observe at the output a sudden increase of the “blue mode” at a location corresponding to the perturbation, correlated with a depression of the “orange mode”; see round trip #1100 in panel (d). We now have a “domain” in which the blue mode dominates embedded within the original orange-dominated state. In that domain, the power levels of the two polarization modes have essentially been interchanged, reflecting the mirror symmetry of the system. This symmetry can be further appreciated by noting that the color plots of the two polarization components measured throughout the experiment [Figs. 3(a) and (b)] are essentially negative images of each other. Correspondingly, the total output power [Fig. 3(c) and black curves in panel (d)] reveals little sign of the polar-

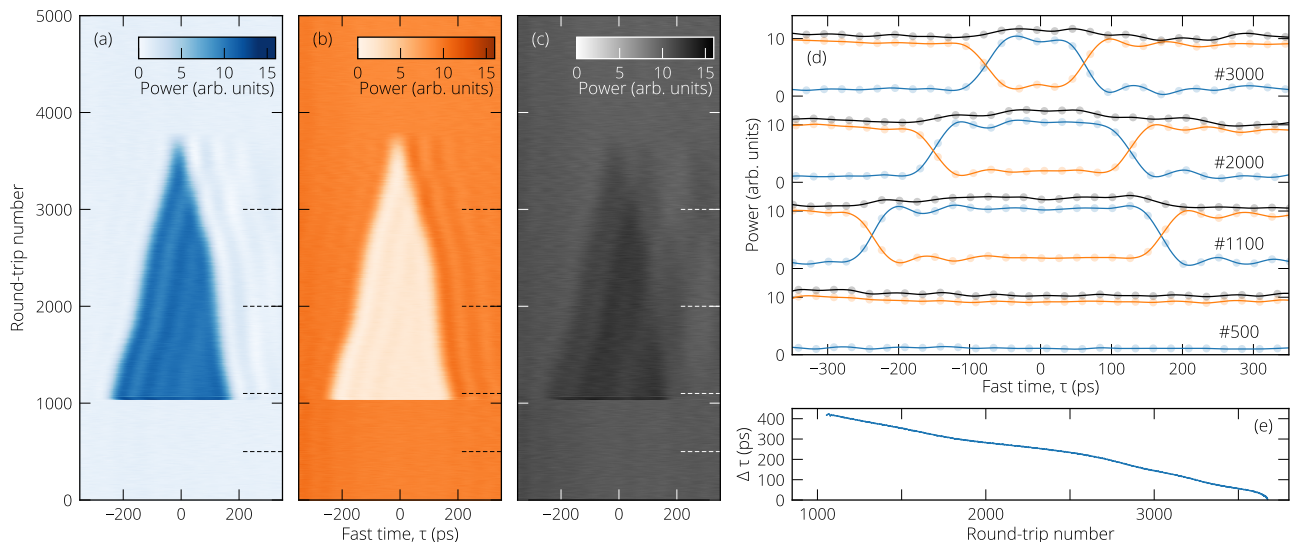


FIG. 3. Experimental evidence of dissipative PDWs for $X \simeq 30.5$ and $\Delta \simeq 13.5$. (a)–(c) Round-trip-by-round-trip evolution of the fast-time output power profile for the two polarization components, $|E_{1,2}(\tau)|^2$ [(a), blue, and (b), orange] as well as for the total signal [(c), grey] before and after a short, localized, 400 ps-long polarization perturbation is applied at about round-trip #1000. The perturbation generates a “blue”-mode dominated domain connected to the surrounding regions by two PDWs. The PDWs drift towards each other, eventually mutually annihilating. (d) provides corresponding line plots using matching colors for selected round-trips as indicated (and marked as dashed side-lines in (a)–(c)). (e) Evolution of the temporal separation $\Delta\tau$ between the PDWs.

ization structure of the intracavity field. We clearly are in presence of an almost pure polarization dynamics.

We identify the transition regions, along the fast-time (τ) coordinate, where the field switches polarization as two PDWs of opposite symmetry. The evolution shown in Fig. 3 reveals that these PDWs slowly drift towards each other (at a rate of about $0.15 \text{ ps}/t_R$); see also panel (e) where we plot the temporal separation between the PDWs vs round-trip number. This results in the shrinkage of the blue-mode dominated domain created by the polarization perturbation. The PDWs eventually collide and mutually annihilate (around round trip #3800), reverting the system to its initial state. If the interchange symmetry between the polarization modes was perfect, the PDWs would have no preferred direction of motion and would remain still (if away from other PDWs). We can therefore attribute the PDWs’ motion to the presence of residual asymmetries, favoring one state over the other [33]. In particular, from the slight excess power visible in the central domain [Fig. 3(c)], we can infer that the blue mode may have been driven slightly stronger than the orange mode. Nevertheless, the PDWs are very robust: they persist for nearly one thousand photon lifetimes while maintaining their shape (as far as the 80 ps temporal resolution of our real-time oscilloscope allows us to judge), demonstrating their dissipative and nonlinearly-localized character.

In order to observe stationary PDWs, we have investigated the use of an external modulation of parameters to trap PDWs, as that technique has been successfully

exploited to pin various types of moving fronts in other nonlinear systems [38–41]. In our case, we modulate the polarization of the driving field, by applying a small fraction of the 10 GHz sinusoidal clock signal to the PM (see Fig. 2). This modulation can be turned on and off with an additional rf switch (SW). Figure 4(a) shows the result of an experiment that starts like that discussed in Fig. 3 (only showing one polarization component), with two PDWs initially drifting towards each other at a constant speed. When the modulation is turned on at round-trip #1200 [see Fig. 4(b) as well as the red-shaded area in Fig. 4(a)], we immediately observe a change of behavior. The PDWs visibly change their drift velocities, and after some transient, eventually reach a fixed position with respect to the modulation. In that position, the PDW drift imparted by the local driving imbalance associated with the modulation counteracts the original motion due to the residual asymmetries. The PDWs hold their position until the modulation is turned off at round-trip #2500, which releases them, back on their original collision course. In Fig. 4(c), using the same technique, we demonstrate long term pinning of two PDWs over 30 seconds (corresponding to a propagation distance of $6 \times 10^6 \text{ km}$ inside the resonator), which has enabled us to measure their temporal intensity profile with a 65-GHz sampling oscilloscope [blue dots in Fig. 4(d)]. This measurement demonstrates that our PDWs have a rise time (10–90%) of less than 9 ps, limited by the bandwidth of our oscilloscope, and compatible with the 1.6 ps numerical expectation [green curves in Fig. 4(d)].

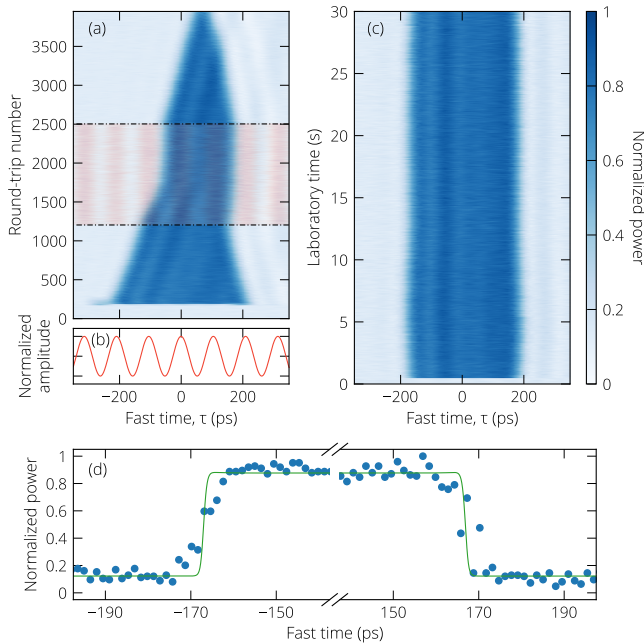


FIG. 4. (a) Demonstration of drifting PDWs being pinned/unpinned to a shallow modulation of the driving polarization. We only show the evolution of the output power of one polarization component. The 10 GHz sinusoidal modulation [transparent shades of red and panel (b)] is applied between round-trips #1200 and 2500. (c) Long term pinning of PDWs, for $X \simeq 24$ and $\Delta \simeq 9.2$. (d) Sampling scope measurement (blue dots) of the temporal intensity profile of the two PDWs trapped in (c). The green curve is the numerical expectation.

We remark that the PDWs reported in Figs. 3 and 4 are observed for driving powers comparatively larger than that considered in the theoretical plot of Fig. 1. Large driving powers are made necessary by the presence of a small amount of linear coupling between the polarization modes of our fiber resonator. Numerical calculations indicate that linear coupling, which splits the cavity resonance [42], thwarts polarization SSB at low power. SSB and PDWs are restored at high power, when the Kerr-induced tilt of the cavity resonance dominates over the splitting [43].

In conclusion, we have reported here the first experimental demonstration of dissipative PDWs. The PDWs are recirculated in a passive, driven Kerr optical fiber ring resonator. Their existence relies on a symmetry breaking bifurcation and on an interchange symmetry between the two polarization modes of the resonator. Our dissipative PDWs are found to be robust with respect to residual imperfections and asymmetries, and can be pinned to a shallow external modulation. Given their duration, our resonator could hold up to 20,000 PDWs in a cw-driven configuration, which could be achieved by mitigating linear mode coupling as in [33], thus reducing power requirements. Our results suggest that our system could be

used as an all-optical buffer for PDW-based topological bit transmissions [13]. Optical PDWs could also prove useful for the real time stochastic analog simulation of other DW-related phenomena.

We thank Y. Wang for technical help, and F. Leo for fruitful discussions. We acknowledge financial support from The Royal Society of New Zealand, in the form of Marsden Funding (18-UOA-310), as well as James Cook (JCF-UOA1701, for S.C.) and Rutherford Discovery (RDF-15-UOA-015, for M.E.) Fellowships. J.F. thanks the Conseil régional de Bourgogne Franche-Comté, mobility (2019-7-10614).

* s.coen@auckland.ac.nz

- [1] M. Golubitsky, I. Stewart, and D. G. Schaeffer, *Singularities and Groups in Bifurcation Theory: Volume II*, Applied Mathematical Sciences No. 69 (Springer-Verlag, New York, 1988).
- [2] P.-E. Weiss, “L’hypothèse du champ moléculaire et la propriété ferromagnétique,” *J. Phys. Theor. Appl.* **6**, 661 (1907).
- [3] F. Tsitoura, U. Gietz, A. Chabchoub, and N. Hoffmann, “Phase domain walls in weakly nonlinear deep water surface gravity waves,” *Phys. Rev. Lett.* **120**, 224102 (2018).
- [4] L. E. Reichl, *A Modern Course in Statistical Physics*, 4th ed. (Wiley-VCH, 2016).
- [5] S. Coen and M. Haelterman, “Domain wall solitons in binary mixtures of Bose-Einstein condensates,” *Phys. Rev. Lett.* **87**, 140401 (2001); D. M. Stamper-Kurn and M. Ueda, “Spinor Bose gases: Symmetries, magnetism, and quantum dynamics,” *Rev. Mod. Phys.* **85**, 1191 (2013).
- [6] S. Weinberg, *The Quantum Theory of Fields*, Vol. 2 (Cambridge University Press, 1995).
- [7] D. Y. Parpia, B. K. Tanner, and D. G. Lord, “Direct optical observation of ferromagnetic domains,” *Nature* **303**, 684 (1983); J. Unguris, R. J. Celotta, and D. T. Pierce, “Observation of two different oscillation periods in the exchange coupling of Fe/Cr/Fe(100),” *Phys. Rev. Lett.* **67**, 140 (1991).
- [8] D. A. Allwood, G. Xiong, C. C. Faulkner, D. Atkinson, D. Petit, and R. P. Cowburn, “Magnetic domain-wall logic,” *Science* **309**, 1688 (2005); S. S. P. Parkin, M. Hayashi, and L. Thomas, “Magnetic domain-wall racetrack memory,” *ibid.* **320**, 190 (2008); J. A. Currihan-Incorvia, S. Siddiqui, S. Dutta, E. R. Evarts, J. Zhang, D. Bono, C. A. Ross, and M. A. Baldo, “Logic circuit prototypes for three-terminal magnetic tunnel junctions with mobile domain walls,” *Nat. Commun.* **7**, 10275 (2016).
- [9] A. Dutta, G. Aepli, B. K. Chakrabarti, U. Divakaran, T. F. Rosenbaum, and D. Sen, *Quantum Phase Transitions in Transverse Field Spin Models: From Statistical Physics to Quantum Information* (Cambridge University Press, Cambridge, 2015).
- [10] V. E. Zakharov and A. V. Mikhailov, “Polarization domains in nonlinear optics,” *JETP Lett.* **45**, 349 (1987).
- [11] S. Pitois, G. Millot, and S. Wabnitz, “Polarization domain wall solitons with counterpropagating laser beams,”

- Phys. Rev. Lett. **81**, 1409 (1998).
- [12] M. Haelterman and A. P. Sheppard, “Polarization domain walls in diffractive or dispersive Kerr media,” *Opt. Lett.* **19**, 96 (1994); A. P. Sheppard and M. Haelterman, “Polarization-domain solitary waves of circular symmetry in Kerr media,” *ibid.* **19**, 859 (1994).
- [13] M. Gilles, P.-Y. Bony, J. Garnier, A. Picozzi, M. Guasoni, and J. Fatome, “Polarization domain walls in optical fibres as topological bits for data transmission,” *Nature Photon.* **11**, 102 (2017).
- [14] M. Haelterman, “Polarisation domain wall solitary waves for optical fibre transmission,” *Electron. Lett.* **30**, 1510 (1994); M. Haelterman and M. Badolo, “Dual-frequency wall solitary waves for nonreturn-to-zero signal transmission in W-type single-mode fibers,” *Opt. Lett.* **20**, 2285 (1995).
- [15] J. Fatome, F. Leo, M. Guasoni, B. Kibler, M. Erkintalo, and S. Coen, “Polarization domain-wall cavity solitons in isotropic fiber ring resonators,” in *Nonlinear Photonics, NP’2016* (Optical Society of America, Sydney, NSW, Australia, 2016) p. NW3B.6.
- [16] G.-L. Oppo, A. J. Scroggie, and W. J. Firth, “Characterization, dynamics and stabilization of diffractive domain walls and dark ring cavity solitons in parametric oscillators,” *Phys. Rev. E* **63**, 066209 (2001).
- [17] D. V. Skryabin, A. Yulin, D. Michaelis, W. J. Firth, G.-L. Oppo, U. Peschel, and F. Lederer, “Perturbation theory for domain walls in the parametric Ginzburg-Landau equation,” *Phys. Rev. E* **64**, 056618 (2001).
- [18] I. Rabbiosi, A. J. Scroggie, and G.-L. Oppo, “Suppression of spatial chaos via noise-induced growth of arrays of spatial solitons,” *Phys. Rev. Lett.* **89**, 254102 (2002).
- [19] S. Trillo, M. Haelterman, and A. Sheppard, “Stable topological spatial solitons in optical parametric oscillators,” *Opt. Lett.* **22**, 970 (1997); G.-L. Oppo, A. J. Scroggie, and W. J. Firth, “From domain walls to localized structures in degenerate optical parametric oscillators,” *J. Opt. B: Quantum Semiclass. Opt.* **1**, 133 (1999).
- [20] V. B. Taranenko, K. Staliunas, and C. O. Weiss, “Pattern formation and localized structures in degenerate optical parametric mixing,” *Phys. Rev. Lett.* **81**, 2236 (1998); A. Esteban-Martín, V. B. Taranenko, J. García, G. J. de Valcárcel, and E. Roldán, “Controlled observation of a nonequilibrium Ising-Bloch transition in a nonlinear optical cavity,” *ibid.* **94**, 223903 (2005).
- [21] Z. Wang, A. Marandi, K. Wen, R. L. Byer, and Y. Yamamoto, “Coherent Ising machine based on degenerate optical parametric oscillators,” *Phys. Rev. A* **88**, 063853 (2013); A. Marandi, Z. Wang, K. Takata, R. L. Byer, and Y. Yamamoto, “Network of time-multiplexed optical parametric oscillators as a coherent Ising machine,” *Nature Photon.* **8**, 937 (2014).
- [22] T. Inagaki, Y. Haribara, K. Igarashi, T. Sonobe, S. Tamate, T. Honjo, A. Marandi, P. L. McMahon, T. Umeki, K. Enbutsu, O. Tadanaga, H. Takenouchi, K. Aihara, K.-i. Kawarabayashi, K. Inoue, S. Utsunomiya, and H. Takesue, “A coherent Ising machine for 2000-node optimization problems,” *Science* **354**, 603 (2016).
- [23] Q. L. Williams, J. García-Ojalvo, and R. Roy, “Fast intracavity polarization dynamics of an erbium-doped fiber ring laser: Inclusion of stochastic effects,” *Phys. Rev. A* **55**, 2376 (1997).
- [24] H. Zhang, D. Y. Tang, L. M. Zhao, and X. Wu, “Observation of polarization domain wall solitons in weakly birefringent cavity fiber lasers,” *Phys. Rev. B* **80**, 052302 (2009).
- [25] C. Lecaplain, P. Grelu, and S. Wabnitz, “Polarization-domain-wall complexes in fiber lasers,” *J. Opt. Soc. Am. B* **30**, 211 (2013).
- [26] L. A. Lugiato and R. Lefever, “Spatial dissipative structures in passive optical systems,” *Phys. Rev. Lett.* **58**, 2209 (1987).
- [27] M. Haelterman, S. Trillo, and S. Wabnitz, “Polarization multistability and instability in a nonlinear dispersive ring cavity,” *J. Opt. Soc. Am. B* **11**, 446 (1994).
- [28] E. Averlant, M. Tlidi, K. Panajotov, and L. Weicker, “Coexistence of cavity solitons with different polarization states and different power peaks in all-fiber resonators,” *Opt. Lett.* **42**, 2750 (2017).
- [29] A. U. Nielsen, B. Garbin, S. Coen, S. G. Murdoch, and M. Erkintalo, “Coexistence and interactions between nonlinear states with different polarizations in a monochromatically driven passive Kerr resonator,” *Phys. Rev. Lett.* **123**, 013902 (2019).
- [30] G. P. Agrawal, *Nonlinear Fiber Optics*, 5th ed. (Academic Press, 2013).
- [31] A. E. Kaplan and P. Meystre, “Directionally asymmetrical bistability in a symmetrically pumped nonlinear ring interferometer,” *Opt. Commun.* **40**, 229 (1982); I. P. Areshchev, T. A. Murina, N. N. Rosanov, and V. K. Subashiev, “Polarization and amplitude optical multistability in a nonlinear ring cavity,” *ibid.* **47**, 414 (1983).
- [32] M. T. M. Woodley, J. M. Silver, L. Hill, F. Copie, L. Del Bino, S. Zhang, G.-L. Oppo, and P. Del’Haye, “Universal symmetry-breaking dynamics for the Kerr interaction of counterpropagating light in dielectric ring resonators,” *Phys. Rev. A* **98**, 053863 (2018).
- [33] B. Garbin, J. Fatome, G.-L. Oppo, M. Erkintalo, S. G. Murdoch, and S. Coen, *Asymmetric Balance in Symmetry Breaking*, accepted in *Phys. Rev. Res.* (2020), arXiv 1904.07222.
- [34] F. Leo, S. Coen, P. Kockaert, S.-P. Gorza, Ph. Emplit, and M. Haelterman, “Temporal cavity solitons in one-dimensional Kerr media as bits in an all-optical buffer,” *Nature Photon.* **4**, 471 (2010).
- [35] A. J. Barlow, J. J. Ramskov-Hansen, and D. N. Payne, “Birefringence and polarization mode-dispersion in spun single-mode fibers,” *Appl. Opt.* **20**, 2962 (1981).
- [36] M. Anderson, F. Leo, S. Coen, M. Erkintalo, and S. G. Murdoch, “Observations of spatiotemporal instabilities of temporal cavity solitons,” *Optica* **3**, 1071 (2016).
- [37] S. Coen, M. Haelterman, Ph. Emplit, L. Delage, L. M. Simohamed, and F. Reynaud, “Experimental investigation of the dynamics of a stabilized nonlinear fiber ring resonator,” *J. Opt. Soc. Am. B* **15**, 2283 (1998).
- [38] N. N. Rozanov, V. E. Semenov, and G. V. Khodova, “Transverse structure of a field in nonlinear bistable interferometers. I. Switching waves and steady-state profiles,” *Sov. J. Quantum. Electron.* **12**, 193 (1982), translated from *Kvantovaya Elektron.* (Moscow) **9**, 354-360 (Feb. 1982); S. Coen, M. Tlidi, Ph. Emplit, and M. Haelterman, “Convection versus dispersion in optical bistability,” *Phys. Rev. Lett.* **83**, 2328 (1999).
- [39] Y. Pomeau, “Front motion, metastability and subcritical bifurcations in hydrodynamics,” *Physica D* **23**, 3 (1986); F. Marino, G. Giacomelli, and S. Barland, “Front Pinning and Localized States Analogues in Long-Delayed Bistable Systems,” *Phys. Rev. Lett.* **112**, 103901 (2014).

- [40] F. Haudin, R. G. Elías, R. G. Rojas, U. Bortolozzo, M. G. Clerc, and S. Residori, “Front dynamics and pinning-depinning phenomenon in spatially periodic media,” *Phys. Rev. E* **81**, 056203 (2010).
- [41] J. K. Jang, M. Erkintalo, S. Coen, and S. G. Murdoch, “Temporal tweezing of light through the trapping and manipulation of temporal cavity solitons,” *Nature Commun.* **6**, 7370 (2015); B. Garbin, J. Javaloyes, G. Tissoni, and S. Barland, “Interaction mediated transport of optical localized states in a trapping potential,” arXiv:1710.01017 (2017).
- [42] J. R. Pierce, “Coupling of modes of propagation,” *J. Appl. Phys.* **25**, 179 (1954).
- [43] L. Del Bino, J. M. Silver, S. L. Stebbings, and P. Del’Haye, “Symmetry breaking of counter-propagating light in a nonlinear resonator,” *Sci. Rep.* **7**, 43142 (2017).